ISSN 0036-0295, Russian Metallurgy (Metally), Vol. 2014, No. 11, pp. 876–887. © Pleiades Publishing, Ltd., 2014.
Original Russian Text © O.K. Belousov, B.P. Mikhailov, N.A. Palii, 2014, published in Metally, 2014, No. 6, pp. 29–42.

On the Role of Acoustic Phonons in Superconductivity

O. K. Belousov, B. P. Mikhailov, and N. A. Palii

Baikov Institute of Metallurgy and Materials Science, Russian Academy of Sciences, Leninskii pr. 49, Moscow, 119991 Russia

e-mail: palii@imet.ac.ru

Received March 27, 2014

Abstract—The macroscopic properties of the elasticity of simple (Nb) and complex ($YBa_2Cu_3O_{7-x}$) superconductors with a high critical temperature T_c are measured and calculated. The longitudinal and transverse acoustic wavelengths are calculated and compared to the lattice parameters and the bond lengths in the superconductors and to some electronic properties. The results of measuring the damping of longitudinal vibrations and calculating the bulk modulus point to significant anomalies at temperatures above the critical temperature.

DOI: 10.1134/S0036029514110020

INTRODUCTION

The key role of phonons in superconductivity was repeatedly noted [1–6]. The appearance of electric fields is related to the energy of elastic waves and wavelengths λ, especially longitudinal tension–compression waves. When in resonance with electromagnetic waves, such waves can cause superpolarizability and an infinitely high permittivity, or superconductivity (as is generally accepted). It should be noted that many authors mentioned that the electron pairing hypothesis can be erroneous [6–8].

The investigation of the phonon–electron interaction performed in this work will help one to approach an understanding of the superconductivity mechanism.

SIMPLE SUPERCONDUCTORS (NIOBIUM)

As was shown in [9], the first and second ionization potentials of elements are close to the kinetic energy of a longitudinal elastic wave, $E_{kin} = M v_{L,0}^2/2$, where M is the atomic mass and $v_{L,0}$ is the longitudinal elastic wave velocity at 0 K (cm/s). For example, the first ionization potential of niobium ($I_1 = 6.77$ eV/at) almost coincides with E_{kin}, and velocity $v_{L,0}$ is expressed as $(E_Y/\rho)^{1/2}$, where E_Y is Young's modulus (GPa) and ρ is the density (g/cm^3). We have $E^0_{kin,Y} = 6.73$ eV/at (difference is 0.6%). Longitudinal wave velocity $v_L = \left(\frac{B + 4/3G}{\rho}\right)^{1/2}$, where B and G are the bulk modulus and the shear modulus, respectively, determines the second ionization potential of niobium ($I_2 = 13.82$ eV/at), and we have $E^0_{kin,Y} = 13.26$ eV/at (difference is ~4%). Using the data on Fermi energy E_F [9] determined from a renormalization condition [6], we calculated the frequency related to an electromagnetic wave, $\nu_{el} = E_F/h = 2.26 \times 10^{15}$ s^{-1}, where h is Planck's constant. Then, the electromagnetic wavelength is $\lambda_{el} = v_F/\nu_{el} = 11.59 \times 10^{-8}$ cm. It is known that the maximum of the electromagnetic energy density is located at $\lambda_{el}/4$; in our case, it corresponds to a distance of 2.898×10^{-8} cm. This distance is close to $2r_{Nb}$ (2.86–2.92 for a coordination number (CN) of 8) and to the interatomic distance in the niobium lattice $a' = a\sqrt{3}/2 = 2.853$ Å (⟨110⟩ direction). A strong phonon–electron interaction can be expected at this distance.

The anomaly preceding the superconducting transition in niobium, i.e., a lattice instability in the ⟨110⟩ direction (⟨$00\bar{1}$⟩ polarization), was also detected in its analogs (V, Ta) in a weaker form [10–12].

Since critical temperature T_c for niobium is 9.301 K for a single crystal, 9.26–9.29 K for a polycrystal, and ~10.7 K at a high pressure [13], it is interesting to study the elastic behavior of pure polycrystalline niobium and to compare it with certain data for single-crystal niobium. Note that the critical temperature of niobium in the nanocrystalline state (thin nanowires) changed weakly: it even decreased to $T_c \approx 6$ K and to $T_c = 2$ K in a field of 11 T [14].

A 100 × 10-mm niobium sample for studying the elastic properties was fabricated from a rod grown upon electron-beam melting and heat treated in vacuum according to the following schedule: heating to 900°C, holding for 3 h, and furnace cooling.

The measurements were carried out on an Elastomat device in the temperature range 295–77 K in cooling and 295–625 K in heating. The vibration damping was measured at longitudinal frequencies

and was expressed in percentage. The initial values at 295 K were $E_Y = 109.9$ GPa and $G = 39.6$ GPa; that is, the Poisson ratio was $\mu = 0.39$ and the damping constant was $\Delta = 0.07\%$. This is a rather high value of μ: it is close to the value of the solid phase near the phase-transition points in the metal, including melting, and characterizes a significant anisotropy, which also determines the electronic behavior of niobium [15–17]. The elastic anisotropy coefficient of niobium is $A = c'/c_{44} = 1.95$, where c' and c_{44} are the microelastic constants (GPa).

Using the temperature dependences of the elastic and electron wavelengths in niobium, the authors of [9] showed the possibility of their resonance and, hence, the generation of persistent currents in the superconductor near T_c of niobium.

The idea of the quantum-mechanical resonance of covalent bonds, as applied to superconductivity, was proposed by Pauling [2, 3]. However, he did not consider the resonance of elastic and electron waves: he only assumed that superconductivity occurs via a phonon–electron interaction.

As was noted in [9], the anomalies in the dependence of the frequency spectrum of vibrations of single-crystal niobium on wavevector q also manifest themselves in the temperature dependence of elastic constant c_{44} in the form of a gentle minimum at ~450 K [12]. As follows from the results of that work, this minimum is also observed for polycrystalline niobium in approximately the same temperature range, and it is less pronounced in the curve of shear modulus (Fig. 1).

This dependence can follow from the Voigt–Reuss–Hill (VRH) approximation, which takes into account the contribution of each microscopic constant [18]. For example, according to Voigt, crystalline grains in a polycrystal undergo the same elastic deformation and the contribution of constant c_{44} is significant. In this case, for Young's modulus we have

$$E_Y^F = \frac{(c_{11} - c_{12} + 3c_{44})(c_{11} + 2c_{12})}{2c_{11} + 3c_{12} + c_{44}}. \quad (1)$$

The Poisson ratio is high over the entire temperature range (see Fig. 1). Its estimation from the microconstants results in the following expression at absolute zero [19]:

$$\mu^0 = c_{12}^0/(c_{L,ij}^0 + c_{12}^0). \quad (2)$$

If $c_{\langle 111\rangle}^0 = 215.26$ and $c_{12}^0 = 133.98$ GPa [18], we have $\mu^0 = 0.384$. Good results are also obtained when the shear modulus at 0 K is estimated from the microelastic constants [18]. In the VRH approximation, we obtain $G^0 \approx 40.47$ GPa at $c_{11}^0 = 254.22$, $c_{12}^0 = 133.98$, and $c_{44} = 30.90$ GPa (see Fig. 1).

Bulk modulus B and its reciprocal quantity, compressibility, play a significant role in the superconductivity mechanism. Using the microelastic constants, we have [18]

$$B = E_Y/3(1 - 2\mu). \quad (3)$$

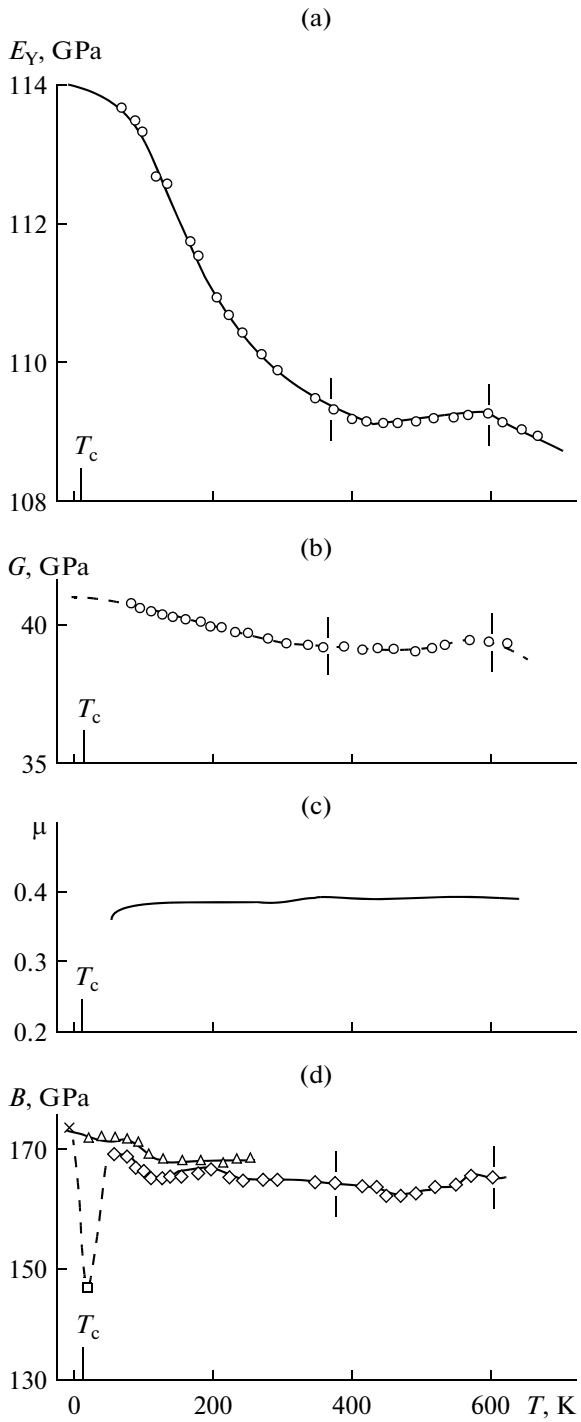

Fig. 1. Temperature dependences of (a) Young's modulus E_Y, (b) shear modulus G, and (c) Poisson ratio μ for polycrystalline niobium and (d) bulk modulus B for high-purity niobium: (△) calculation from microconstants for single crystals [12], (◇) the same for polycrystal, (□) the same for extrapolation to 9 K, and (×) calculation by Eqs. (3) and (4).

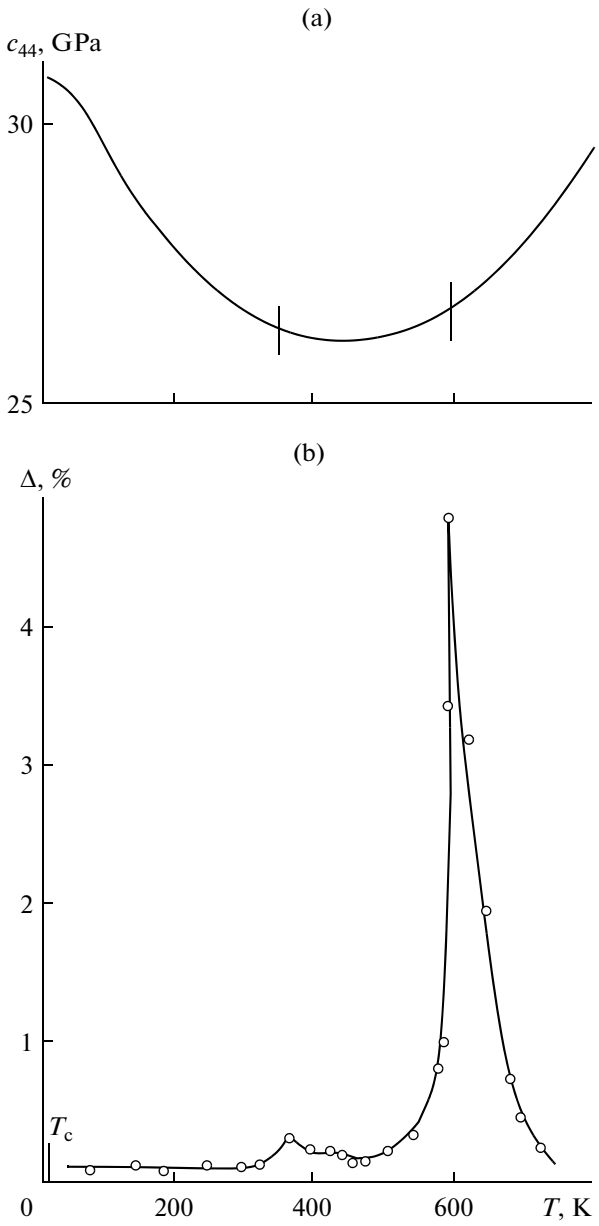

Fig. 2. Temperature dependences of (a) elastic constant c_{44} of niobium (single crystal) [12] and (b) damping constant Δ of longitudinal vibrations in niobium (polycrystal).

With Eqs. (1) and (2), at absolute zero we can write

$$B^0 = 1/3(c_{11}^0 + 2c_{12}^0), \quad (4)$$

i.e., $B^0 = 174$ GPa (point × in Fig. 1d). In the B curve plotted from the data in [12], a weak decrease is seen beginning from ~100 K and the calculated values of B are then close to those measured on polycrystalline niobium in that work. However, the authors of [12] did not analyze the transition from 10 K down, i.e., from the normal to the superconducting phase of niobium. Having no possibilities to perform measurements in this temperature range, we extrapolated the elastic vibration frequencies to this range and obtained the following result. The elastic constants near T_c are $E_{Y, T_c} = 114$ GPa and $G_{T_c} = 41.57$ GPa; as a result, the Poisson ratio is $\mu_{T_c} = (E_Y/2G) - 1 = 0.371$. Here, we have $B = 147.3$ GPa (Fig. 1d, square point). Thus, the transition of niobium into the superconducting state at 10 K or below is likely to be related to an increase (softening) and subsequent decrease of compressibility χ (stiffness), which is likely to be part of the mechanism of transition of the normal metal into superconductor. Comprehensives measurements are to be performed in this temperature range. The results of measurements performed at 77 K indicate a certain decrease of μ (see Fig. 1c).

Figure 2 shows the temperature dependence of constant c_{44} (single crystal) and damping Δ at the longitudinal natural oscillation frequencies (polycrystalline sample). The strong peak of Δ corresponds to ~600 K and the weak peak, to 360 K. The peak temperatures correspond to the decrease of the $c_{44}(T)$ curve on either side of the gentle minimum (~450 K), which is also characteristic of the polycrystal (Figs. 2a, 2b). Constant c_{44} continues to grow upon heating up to 2500 K [12], whereas macroscopic moduli E and G decrease uniformly above 600 K (see Fig. 1). The damping peaks (internal friction) in Fig. 2 point to the structural instability of niobium that precedes the phase transition at T_c. From a theoretical standpoint, another peak, which is related to the transition below 10 K, should exist, and its detection needs investigations at lower temperatures.

Thus, using niobium as an example, we showed that the anomalies of its elastic spectrum manifest themselves in the E_Y, G, Δ, and B curves, including the polycrystalline state of the material [9].

The calculation of the electron and acoustic wavelengths indicates that a resonance between them is possible (Fig. 3) [9]. This resonance enhances the instability effect provided that the defect concentration is significant: it leads to an irreversible change in the bond lengths and the bond angles. This instability precedes the transformation of the substance into superconductor, which was repeatedly noted by researchers. These concepts can also be applied to amorphous substances, which have free volume related to a high defect concentration increasing T_c.

The longitudinal acoustic wavelengths or their multiple lengths become comparable with the interplanar spacings, i.e., the shortest interatomic distances, which ensures the interaction of phonons with the electron charges connecting atoms. At a certain degree, this specific feature also reflects the concept of resonating bonds in a substance, e.g., an electron pair coupling resonance [2, 3]; however, in the case of superconductivity, it should be preceded by the reso-

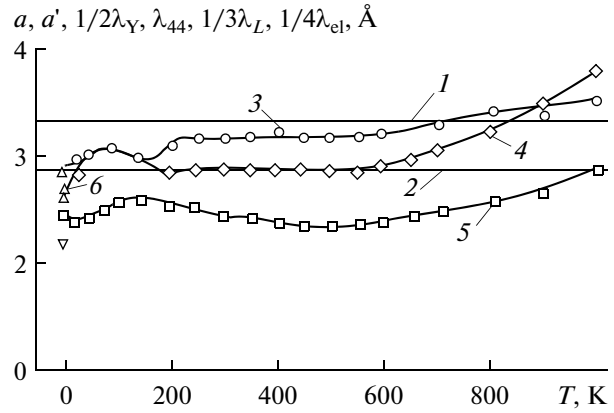

Fig. 3. Temperature dependences of the elastic and electron wavelengths in niobium: (*1*) lattice parameter a (Å), (*2*) $a' = a\sqrt{3}/2$, (*3*) $1/2\lambda_Y$, (*4*) λ_{44}, (*5*) $1/3\lambda_L$, and (*6*) $1/4\lambda_{el}$ [9].

nance (or synchronization) of acoustic and electron waves.

This transition should be accompanied by a decrease in volume and an increase in stiffness down to very low temperatures.

COMPLEX SUPERCONDUCTORS (HIGH-T_c SUPERCONDUCTORS (HTSCs))

After the discovery of lanthanum-based ceramic HTSCs in 1986, many researchers studied the elastic constants in yttrium ceramic $YBa_2Cu_3O_{7-x}$ and the temperature anomalies in the temperature range from T_c to 300 K. Although an electron–phonon interaction is considered to be the main factor influencing the stability of such materials and the appearance of superconductivity, its role and, especially, the driving forces are still unknown [20].

Since most earlier works do not present the absolute values of the elastic constants, which are necessary to calculate may properties, and only give their relative values for the limited temperature range 4.2–300 K [21–23], we present the results of measurements in a wider temperature range from 77 to 800 K in order to understand and calculate the elastic energy, acoustic wavelength λ, and the Debye frequency.

Experiments were carried out on an yttrium ceramic sample of sizes L = 76.33 mm and d = 11.98 mm. The sample density at 293 K was $\rho = 5.582$ g/cm^3 (tabulated density is $\rho = 5.72$ g/cm^3).

It should be noted that ceramic HTSCs, in particular yttrium HTSCs, have a martensitic twinned structure [23], and they exhibit the pseudoelasticity characteristic of metallic shape-memory alloys [24].

The absolute values of the elastic constants of yttrium ceramic HTSCs depend strongly on the heat-treatment conditions, the oxygen content, and the content of the nonsuperconducting tetragonal phase

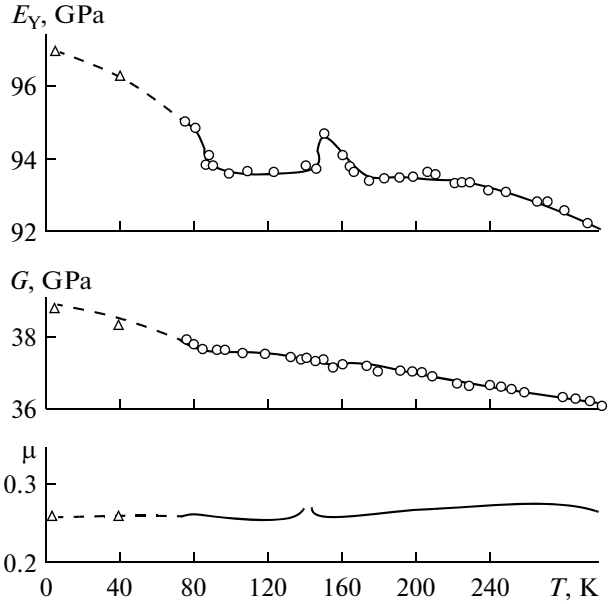

Fig. 4. Changes of Young's modulus, the shear modulus, and the Poisson ratio of yttrium ceramic $YBa_2Cu_3O_{7-x}$ in the temperature range 0–300 K: (△) data from [21–23] for 4.2 and 40 K and (○) measurement results.

(i.e., the ratio of its content to the superconducting orthorhombic phase content). Therefore, Young's modulus at 293 K can vary in the range 91–102 GPa and can be even higher (E_Y = 110–150 GPa [23]), although these differences are incompletely understood.

Figure 4 shows the results of measuring E_Y and G by a dynamic method in the temperature range 295–77 K, i.e., upon cooling. Using these data, we calculated the Poisson ratio and bulk modulus B.

The initial value of Young's modulus at 295 K is E_Y = 91.72 GPa. Cooling to 210 K led to a certain increase of E_Y, which then changes weakly. However, an anomaly related to an increase of E_Y to 94.8 GPa is detected in the temperature range 175–150 K. The segment in the range 150–100 K is almost linear with $E_Y \approx 94$ GPa. E_Y begins to grow sharply at ~90 K and it grows more smoothly from ~83 K. Upon cooling from 295 to 160 K, shear modulus G increases almost linearly, a certain convexity toward the ordinate axis appears to ~90 K, and a sharper increase takes place upon cooling to 77 K. The Poisson ratio at 295 K is μ = 0.25. At low temperatures, it is close to 0.26–0.25, which is in agreement with other reported data. For example, the authors of [21] presents μ = 0.29 for yttrium ceramics with E_Y = 90.8 GPa; in other samples of such ceramics (E_Y = 101.8 GPa), we have μ = 0.198, which is close to 0.20.

In the temperature range from 160 to 280 K, μ increases significantly (to 0.28 or higher) and then again decreases. A less pronounced anomaly was detected in the transition range. As will be shown

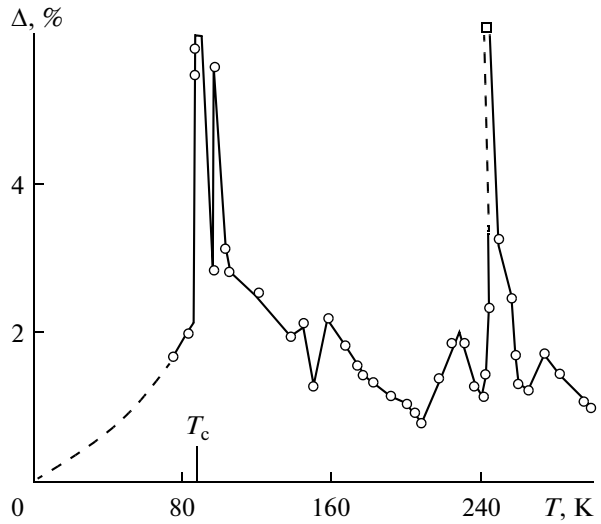

Fig. 5. Temperature dependence of the damping constant of longitudinal vibrations in ceramic $YBa_2Cu_3O_{7-x}$: (---) possible change of the damping constant below T_c, (□) the same for torsional vibrations, and (–○–) measurement results.

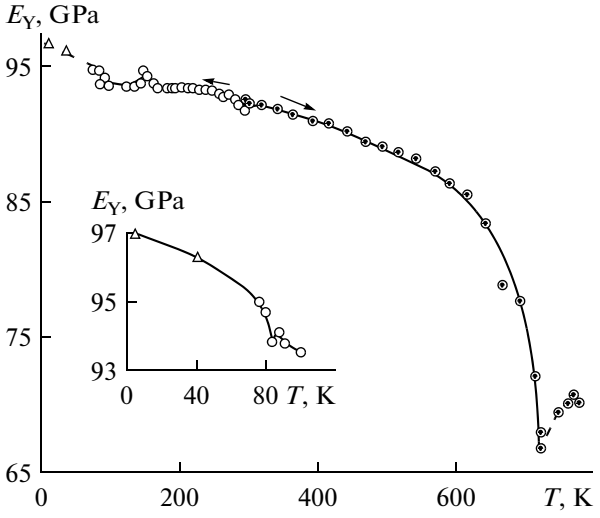

Fig. 6. Temperature dependence of Young's modulus for the perovskite structure of $YBa_2Cu_3O_{7-x}$ in the range 0–800 K. In inset, the range 0–100 K.

below, this behavior strongly affects bulk modulus B, since μ is used for its calculation (see Eq. (3)). The anomaly of μ (in arbitrary units) was also noted in [23].

Figure 5 shows the results of measuring damping constant Δ upon cooling in the temperature range under study in percentage. This dependence has a complex character, which reflects the processes that occur in yttrium ceramic in this temperature range [20–29]. For example, damping anomalies were detected at ~70–125 K [25]. In [28], internal friction peaks were detected at ~110 and 230 K, and the peak intensities decreased with decreasing oxygen content in a sample with an orthorhombic structure and disappeared in a sample with a tetragonal (nonsuperconducting) structure. Nevertheless, the peaks at 88 and 260 K did not change when the oxygen stoichiometry changed. It was noted that the peaks at 88 and 100 K characterize the relaxation processes that are related to the Cu(1)–O(1) (i.e., axis a of the orthorhombic lattice) atomic chains and the peak at 88 K characterizes the processes related to the Cu(2)–O(2) (axis c) chains. The peak the onset of which corresponds to ~260 K can be associated with oxygen deficiency (phase transition; see Fig. 5). The authors of [27] detected three damping peaks at 80, 170, and 210 K (these peaks also correlated with the changes of the shear wave velocity), and the authors of [30] described damping at longitudinal and transverse frequencies and a temperature of ~220 K and noted that the corresponding peak reflects a structural order–disorder transition. The effects related to the redistribution of oxygen cations and atoms during the structural disordering in $YBa_2Cu_3O_{6.93}$ ceramic and the influence of the grain size on this disordering were revealed in [31]. Moreover, a diamagnetic signal, which corresponds to temperature T_c^{max} (~92 K) of this ceramic, was detected. This temperature agrees well with the temperature ($T_c^{calc} = 92.5$ K) calculated in [9].

The damping peaks in Fig. 5 correspond to 89, 104, 226, and 250 K, the initial value of Δ tends to increase up to T_c, and an anomaly is visible at 150 K (it correlates with the anomaly of E_Y in Fig. 4). Below T_c, Δ decreases gradually down to 77 K. Its further possible decrease (dashed line) also correlates with the reported data (see, e.g., [9]). This part of the damping curve (below T_c) is likely to be described similarly to the curve plotted using the measured values of damping constant, e.g., for tin for the Bardeen–Cooper–Schrieffer (BCS) or the Bragg–Williams calculation [9]. However, the choice of the order parameter is not obvious and the measurements should be performed down to 4.2 K.

In this work, Young's modulus was measured upon heating of the described yttrium HTSC sample in a Förster furnace in an air atmosphere from 293 to ~800 K at a heating rate of ~20°C/min (Fig. 6).

The character of curve is analogous to that during an order–disorder transition in, e.g., brasses [32], where it is controlled by elastic energy to a certain temperature. The critical transition point is $T_c' \approx$ 720 K (447°C) and we have $E_{Y, T_c'} = 67–68$ GPa (see Fig. 6). For β brass, we have $T_c' = 727$ K at $E_{Y, T_c'} =$ 70 GPa (another value is $T_c' = 736$ K (463°C) [33]).

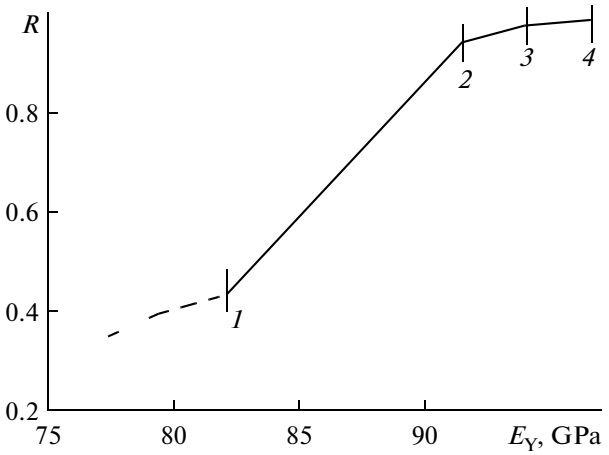

Fig. 7. Young's modulus vs. order parameter R (Bragg–Williams approximation) for $YBa_2Cu_3O_{7-x}$ HTSC in the temperature range 0–648 K: (*1*) $T/T_c' = 0.9$ (648 K), (*2*) 0.42 (302 K), (*3*) 0.12 (83 K), and (*4*) 0.

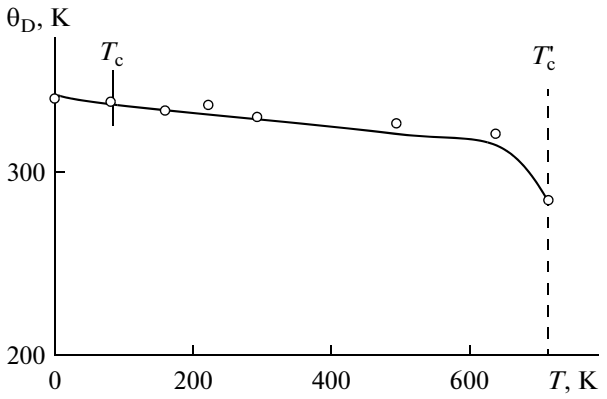

Fig. 8. Change of Debye temperature θ_D of $YBa_2Cu_3O_{7-x}$ in the temperature range 0–720 K.

It is possible that, in the case of HTSC, copper atoms and their partial transition from the divalent into the univalent state in disordering play a key role. Then, using the dependence of order parameter R on reduced temperature T/T_c' we can plot E_Y versus R (Fig. 7). The revealed linear dependence of E_Y on order parameter R corresponds to the temperature ranges 0–83, 83–302, and 302–648 K. In other words, the order–disorder process is controlled by elastic energy in the temperature range 0–648 K, and diffusion processes are likely to be predominant above 648 K. This curve can also explain the anomalous behavior of the properties of the ceramic in the temperature range 300–90 K, where processes have a shear character, which manifests itself in the microstructure of twins [23].

The temperature dependence of E_Y in the range below T_c belongs to the normal phase–superconducting phase transition (inset to Fig. 6), and the order parameter can be represented by, e.g., Landau displacement u_i, i.e., $\lambda = u_i/a$, where a is the lattice parameter [34]. This displacement can be caused by the phase transition, which determines both lattice softening and the character of anharmonic vibrations.

This approach is likely not to be approached to all substances: for example, superconducting tungsten has $T_c = 0.012$–0.015 K and is elastically isotropic down to temperatures close to 0 K, and the elastic anisotropy coefficient is $A = 1$ for the estimation at $T = 0$ K [18]. Obviously, the surface should be considered as a macrodefect in this case, and the elastic wavelengths should be calculated for the case of so-called Rayleigh surface waves [35].

Figure 8 shows the variation of Debye temperature θ_D of the yttrium ceramic calculated from the measured elastic constants in the temperature range 0–720 K. This dependence is close to a linear function up to ~648 K and then decreases sharply: $\theta_D^0 = 346$ K at absolute zero, 338 K at T_c, 320 K at 648 K, and 276 K at T_c'. The value calculated in [23] from the elastic constants is $\theta_D = 344$ K, and this temperature for the yttrium ceramic according to [9] is $\theta_D^0 = 345$ K.

We now apply the relaxation concepts developed by Zener and Ke Tinsui and generalized to metals and their alloys in [36] to $YBa_2Cu_3O_7$. When calculating, e.g., $E_{Y,\,rel}$ and G_{rel}, we can estimate the relaxation Debye frequency at $T_c = 90$ K ($\theta_{D,rel,90} = 271$ K). This temperature differs from $\theta_{D,\,T_c'} = 276$ K for the disordering point by approximately 2%.

Thus, the conditions that correspond to the disordered state of the ceramic structure and the related characteristics of phonons (wavelength, frequency) can appear during relaxation vibrations. These conditions can result in the resonance of elastic and electron waves [9]. Such vibrations are considered as time-dependent imperfections, and they play a key role in superconductivity [37]. Moreover, they cause the damping of ultrasonic waves near T_c. As noted above, the elastic anomalies are most pronounced in the temperature range 80–300 K, i.e., in the range where diffusion processes in ordering are retarded and longitudinal elastic modulus E_L and related longitudinal waves (tension–compression waves), which are sensitive to such anomalies, play a key role [27–29]. The main factor here is bulk modulus B, since we have

$$E_L = B + 4/3G. \quad (5)$$

The quantity that is reciprocal to B (compressibility χ) is known to determine thermal expansion, and bulk

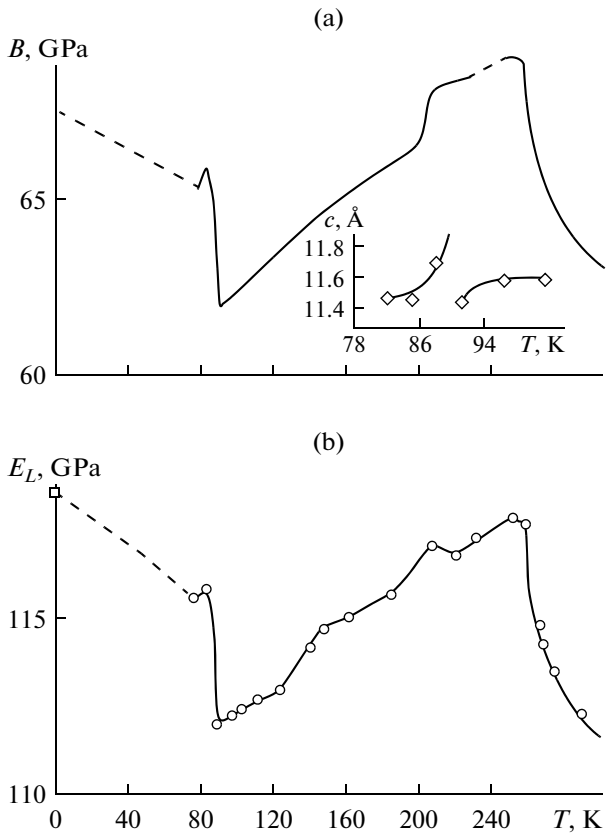

Fig. 9. Temperature dependences of (a) bulk modulus B and (b) longitudinal elastic modulus E_L in the range 0–300 K for ceramic $YBa_2Cu_3O_{7-x}$. In inset, the change of lattice parameter c of the ceramic in the $n \rightarrow s$ transition range [39].

modulus is determined as the second derivative of energy with respect to displacement,

$$B = -\frac{R_0^2}{2}\partial^2\frac{E_{coh}}{\partial R^2}\bigg|_{R-R_0}, \qquad (6)$$

where R_0 is the equilibrium state and E_{coh} is the binding energy.

Figure 9a shows the change of B calculated by Eq. (3) for the temperature range under study. The complex character of the curve reflects the processes related to internal friction (see Fig. 5) [20, 23, 26–31, 38]. The anomalies of B depend strongly on a change of the Poisson ratio (see Eq. (3)) [23]. The sharp increase of modulus B, its subsequent decrease to a minimum at about 90 K (T_c) (compressibility increases here), the sharp increase in the segment to 83 K, and smother increase to 0 K (dashed segment, estimated value is shown by the triangle point) reflect a decrease in compressibility (stiffness). The rectification of such curves using, e.g., the data obtained by a pulsating echo method at frequencies from 10 to 30 MHz gives a significant discrepancy between these results and the results obtained by, e.g., a direct measurement of the frequencies of natural vibrations.

The inset to Fig. 9a shows the change of parameter c of the perovskite lattice in the $n \rightarrow s$ phase transition range. The X-ray diffraction pattern corresponded to an orthorhombic structure, and lattice parameters a and b changed only weakly in this case [39]. The sharp increase of this parameter led to a noticeable change in the unit cell volume from ~169.5 to ~178 Å^3. Therefore, the phase transition in the HTSC under study cannot be attributed to a second-order phase transition, since it has signs of first- and second-order phase transitions.

The curves in Figs. 9a and 9b are similar, the change of longitudinal elastic modulus (Fig. 9b) calculated by Eq. (5) is analogous to the change of bulk modulus B (Fig. 9a), and it is clearly visible that the $n \rightarrow s$ transition in HTSC proceeds with preliminary softening of the orthorhombic modification of perovskite.

It should be noted that the $n \rightarrow s$ transition is characterized by a hysteresis upon heating and cooling. In this case, the elastic moduli (especially B) and the Poisson ratio exhibit significant changes in the range ~250–90 K (T_c) upon cooling and in the range 170–300 K upon heating, and the transition point (T_c) is not revealed upon heating [40].

Neutron diffraction of $YBa_2Cu_3O_{7-x}$ demonstrates the presence of a perovskite structure with oxygen deficiency. At a low oxygen content (e.g., O_6), the structure transforms into the tetragonal (nonsuperconducting) structure. This transformation can also be achieved upon heating (disordering). As is seen from Fig. 6, Young's modulus of the material increased to E_Y = 98.2 GPa after heating to ~800 K (527°C) followed by cooling to room temperature. After the first week of storage E_Y was 95.4 GPa; after two weeks, E_Y = 95.2 GPa; and after three weeks, E_Y decreased to 94.5 GPa. This behavior demonstrates that reversible processes, which restore the initial state of the alloy, occur in yttrium ceramic at 295 K.

In most works, the stability of the orthorhombic lattice of perovskite is related to the Cu(1)–O and Cu(2)–O bond chains and the corresponding planes [21, 28]. Therefore, bond lengths l can be compared to the longitudinal elastic wavelength $\lambda_L = \nu_L/\nu_D$ calculated in this work. However, one-third of this wavelength is comparable with the Cu(2)–O(4) bond length, which is responsible for the distance along axis c in perovskite (Fig. 10) [21]. This bond length is ~2.306 Å [21, 28]. As is seen from Fig. 10, we have $(1/3)\lambda_L \equiv l$(Cu(2)–O(4)) at point T_c', i.e., at the disordering temperature, where longitudinal wave λ_L is in resonance with this bond. The change of this bond length at temperatures below T_c demonstrates that lattice parameter c, as lattice parameter a, can play a key role in the superconductivity of HTSC.

Another characteristic directly related to interplanar spacing a in the perovskite structure is the Cu(1)–O(1) bond length, which corresponds to $(1/3)\lambda_{E_Y}$, i.e., one-third of the wavelength determined through Young's modulus, and $(2/3)\lambda_{E_Y} = a$, Å (see Fig. 10). This is a very important result. It demonstrates that lattice parameter a is fully controlled by elastic forces over a wide temperature range, the Cu–O bond of the given length has a 47% ionic character, and superconductivity can be achieved in such chains resonating via an interaction with acoustic phonons (i.e., during the transitions of a partly ionic (ionic–covalent) into a metallic bond) [3]. When considering relaxation lattice vibrations and assuming that the equation characteristic of metals and alloys is also valid for the ceramic under study, we can calculate $(1/3)\lambda_L$ at, e.g., point T_c, i.e., for the metal → superconductor phase transition, [36]

$$\nu_{L,\,\mathrm{rel}} = \nu_L^0[(1+\mu)(1-2\mu)/(1-\mu)]^{1/2}, \qquad (7)$$

where $\nu_L^0 = \nu_L$ at T_c. Then, we have $(1/3)\lambda_{L,\,90} = 2.36$ Å (indicated by point ×); that is, a resonance can be achieved at temperature T_c for the bonds directed along axis c in the case of relaxation vibrations. It is interesting that the Debye temperature calculated for this case is $\theta_{D,\,90} = 271$ K, whereas we have $\theta_D = 276$ K at point T_c'. Thus, such vibrations can be related to a reversible order–disorder transition. When the grain size decreases, the positions of oxygen atoms in superconducting layers change significantly [31]. As a result, wavelength λ, the bond lengths, and the bond angles are likely to be changed, which can influence T_c.

We now compare the data of energy calculations obtained from studying the elastic constants in yttrium ceramic to the characteristics of, e.g., free copper oxide Cu–O, where copper is divalent (the same was detected in the O–Cu···O–Cu chain [2, 3]). As noted above, we have $T_c' = 720$ K for yttrium ceramic, which is close to the temperature of disordering of, e.g., brass (736 K) [32, 33]. Thus, we can easily calculate the energy of such a transition using the Bragg–Williams approximation [33]. Assuming $Z = 1$ in the equality $ZV_\varepsilon = 2N_A k_B T_c$, where Z is the number of particles and V_ε is the ordering energy, we have $V_\varepsilon = 11.979$ kJ/mol. It is interesting that this result is close to the enthalpy of melting of copper oxide (11.805 kJ/mol; the discrepancy is 1.5%) [41]. Moreover, CuO decomposes at ~1300 K, which is very close to the melting temperature of pure copper (1357 K), at which the bonds in pure copper break in the amount that is proportional to the change of the volume upon melting [35].

We now calculate the shear elastic energy at the critical point of the $n \to s$ transition; that is, we determine $\varepsilon = M\nu_{t,\,\mathrm{rel},\,T_c}^2$ for relaxed vibrations at critical temperature T_c and perform a similar calculation for

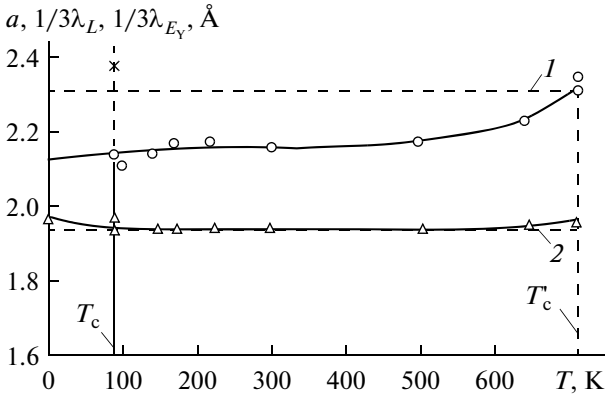

Fig. 10. Temperature dependences of the elastic wavelength calculated from the longitudinal elastic moduli ((○) $1/3\lambda_L$) and Young's modulus (△) $1/3\lambda_Y$) in comparison with bond lengths (*1*) l(Cu(2)–O(4)) ≈ 2.306 Å and (*2*) l(Cu(1)–O(4)) ≈ 1.942 Å. (×) Relaxed value.

T_c', since the difference between the shear moduli for them is small ($G_{T_c,\,\mathrm{rel}} = 24.84$, $G_{T_c'} = 24.53$ GPa). As a result, we have $\varepsilon_{T_c,\,\mathrm{rel}} = 239.611$ kJ/mol and $\varepsilon_{T_c'} = 236.622$ kJ/mol; that is, the shear elastic energies of relaxed shear vibrations at temperatures T_c and T_c' are close to each other. We compare these values with the defect formation energy in CuO using the method proposed in [9], where $H_v = T_m S_m$ is equal to the dissipative part of the free energy of the solid phase at the melting point. For a melting temperature $T_m = 1720$ K and a melting entropy $S_m = 138.14$ J/(mol K), we obtain $H_v = 237.597$ kJ/mol. In both cases, the discrepancy between the values of $\varepsilon_{T_c,\,\mathrm{rel}}$, $\varepsilon_{T_c'}$, and H_v is about 0.6%.

Thus, we can preliminarily conclude that a reversible break of one of the two copper–oxygen bonds in a chain can occur during relaxation vibrations in the structure of HTSC, as was demonstrated in [2, 3]. In this case, the phonon-induced conduction has a metallic type. By analogy with exoelectron emission, it can be attributed to endoelectron emission, which determines persistent currents in the superconductor provided acoustic and electron waves are in resonance [9]. Here, critical temperature T_c is determined by the defect concentration (i.e., the number of broken bonds), i.e., the bonds in which the bond length and the bond angle change during relaxation vibrations.

The table gives the lengths of some interatomic bonds l in the superconducting structure of HTSC presented in Fig. 11a in comparison with the length (or its part) of phonon waves calculated from the macroelastic constants [21, 38]. According to [23], the lattice parameters of the superconducting orthorhombic phase are (Å) $a = 3.8493$, $b = 3.8629$, and $c = 11.6803$. They can slightly vary with temperature: at 740 K

Copper–oxygen bond lengths l as compared to phonon wavelengths λ in the orthorhombic structure of yttrium ceramic $YBa_2Cu_3O_7$

Bond	l, Å	λ, Å	Note
Cu(1)–O(4)	1.843	1.830	$1/2\lambda_i$,
Cu(1)–O(1)	1.942	1.940	$1/3\lambda_{E_Y}$
Cu(2)–O(4)	2.306	2.140	$1/3\lambda_L$
Cu(2)–O(3)	1.958	1.964	$1/3\lambda_{L,\,rel}$

(which is higher than T_c' only by 20 K), we have $a = 1/3c$; that is, the oscillations of these two lattice parameters are synchronized in disordering. This is in agreement with the values of c given in the inset to Fig. 9a.

According to the tabulated data, the Cu(1)–O(1) bond is responsible for axis a of the structure and the Cu(2)–O(4) bond is responsible for the instability along axis c, and its length can be approximately calculated as the sum of the ionic radii of copper (1.57 Å) and oxygen (0.73 Å). We obtain a bond length of 2.30 Å, and this bond can be considered as a metallic–covalent bond. It is interesting that the body force of pinning of polycrystalline yttrium HTSC films at high magnetic fields and a current-carrying ability of $\sim 10^5$ A/cm^2 is determined by shear microconstant c_{66}, which leads to the deformation of a vortex lattice [42]. It is also important how strong the (020) interplanar spacing changes when the majority of oxygen atoms, which are likely to be responsible for the instability of HTSC in the temperature range from T_c to 300 K, are located in such planes (Fig. 11c) [29]. This distance correlates with the longitudinal wavelength calculated from modulus E_Y: $\lambda_{E_{Y,90}} = 5.81$ Å and $\lambda_{E_{Y,90},\,rel} = 5.89$ Å; in essence, it covers all possible distances from 300 K to T_c. These interplanar spacings are very important for the interpretation of the behavior of oxygen and lattice softening above 90 K. The authors of [29] note that this loss of elastic stability plays an important role in superconductivity. For example, we have $b/a = 1$ upon heating to T_c', which is important to obtain high T_c (maximum deviation from tetragonality). Relaxation vibrations can strongly influence the order–disorder transition in the ceramic under study and can support the assumption [3] that conductivity increases due to a resonance in the O–Cu···O–Cu chain, which is achieved through an interaction with phonons.

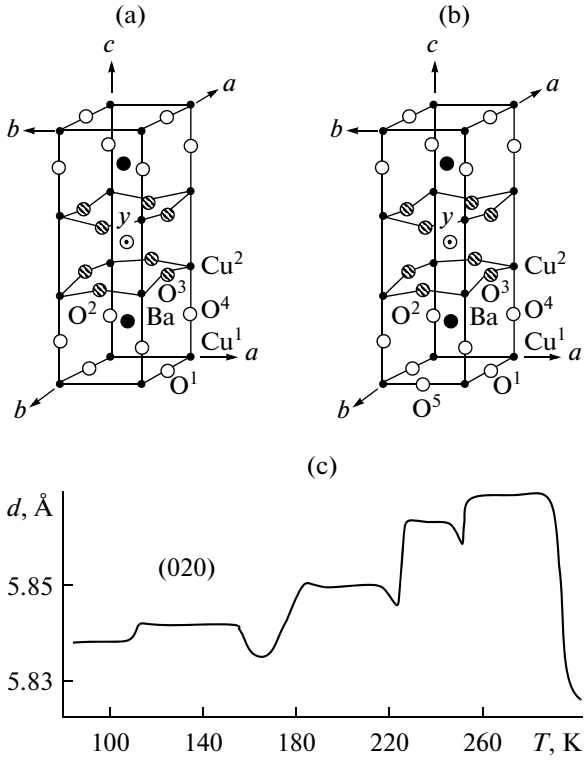

Fig. 11. Crystal structure of $YBa_2Cu_3O_{7-x}$: (a) orthorhombic (superconducting) phase and (b) tetragonal (nonsuperconducting) phase [38]. (c) Change of the (020) interplanar spacing in the temperature range 300–80 K [29].

However, as is seen from the table, the Cu–O bond lengths can vary in the structure of HTSC, and the Cu(2)–O(2) bond (not given in the table) can be considered as an ionic–covalent bond. Its length is 1.929 Å and it can be obtained as the sum of the ionic radius of oxygen (0.73 Å) and the covalent radius of copper (1.17 Å). The bond length of 1.9 Å indicates that bond metallization is unlikely in the Cu(2)–O(2) chain.

Figure 11b shows the structure of the nonconducting tetragonal phase, which forms at high temperatures [38]. In this structure, oxygen occupies site O(5). As noted above, the action of phonons can cause the breakage of one of the covalent copper bonds during relaxation vibrations, which results in the metallization of copper (appearance of conductivity and superconductivity). Energy calculations support this behavior for the characteristics of copper and its oxide. Many facts of changing the electrical conductivity of substances with covalent bonds are known upon melting and some phase transitions. For example, the conductivity of covalent germanium increases in melting, which is associated with metallization, i.e., a change in the character of bonding. In [9], we calculated critical temperature T_c of arsenic and showed that $T_c \approx 50$ K for so-called pnictides, which was detected for doped FeAs compounds.

To support these considerations, we calculate the oscillator energy for temperature T_c', i.e., order–dis-

order transition temperature (720 K), in HTSC with $\theta_{T_c'} = 276$ K,

$$\bar{\varepsilon} = n\left(0.5h\nu + \frac{h\nu}{e^{\beta} + 1}\right), \quad (8)$$

where $n = 1, 2, 3$ (for one-, two-, and three-dimensional oscillators, respectively) and ν is the acoustic frequency that is identical to $\bar{\nu}_D$, i.e., corresponds to Debye temperature $\bar{\theta}_D$, $\beta = \bar{\theta}_D/T$. From Eq. (8), we obtain $\bar{\varepsilon} = 12.126$ kJ/mol at $n = 2$ (two-dimensional oscillator). This value differs from the latent heat of melting of CuO (11.805 kJ/mol), which is related to bond metallization and an increase in the electrical conductivity, only by 2.6%. This finding again demonstrates that the processes of bond breaking and recovery, which generate electromagnetic fields and electric charge waves, can exist in the O–Cu···O–Cu chain during the order–disorder processes induced by resonance reversible atomic vibrations in the HTSC lattice. When HTSC is loaded by an electric current, diffusion processes related to oxygen depletion can occur in it, and excess copper atoms are fixed in stable Cu_2O complexes with a melting (solidification) heat of 56.092 kJ/mol [41], which is fivefold that the melting heat of CuO. In other words, the structure is thermodynamically stable and has high elastic constants ($E_Y \geq$ 150 GPa), as would be expected for oxide systems [18]. In turn, this decreases λ_L, λ_{E_Y}, and λ_t, i.e., the corresponding elastic wavelengths, and increases the frequencies of elastic vibrations, which remove the lattice softening effect before the transformation of the substance in the superconducting state. The superconductivity of this material should degrade in time, which is observed experimentally.

The order–disorder process in the temperature range 293–720 K is rather well understood, but this process in the temperature range 0–90 K is unclear in the sense of choosing an order parameter, which was noted earlier in [43]. On the one hand, the process in this temperature range can be described using the standard Bragg–Williams approximation, as was done for the ultrasound damping curve for tin at temperatures below T_c. The calculated curve agrees with the experimental curve even better than the BCS curve, since the BCS theory has to take into account the change of the energy gap with temperature. Figure 12 shows the results of measuring the upper critical magnetic field H_{c2} of yttrium ceramic with a critical temperature of 60 K [44]. This curve is well described by the Tuin equation for the critical field,

$$H_c(T) = H_c(0)\left[1 - \left(\frac{T}{T_c}\right)^2\right], \quad (9)$$

where $H_c(0)$ is the critical field at 0 K and T_c is the critical temperature of the $n \to s$ transition.

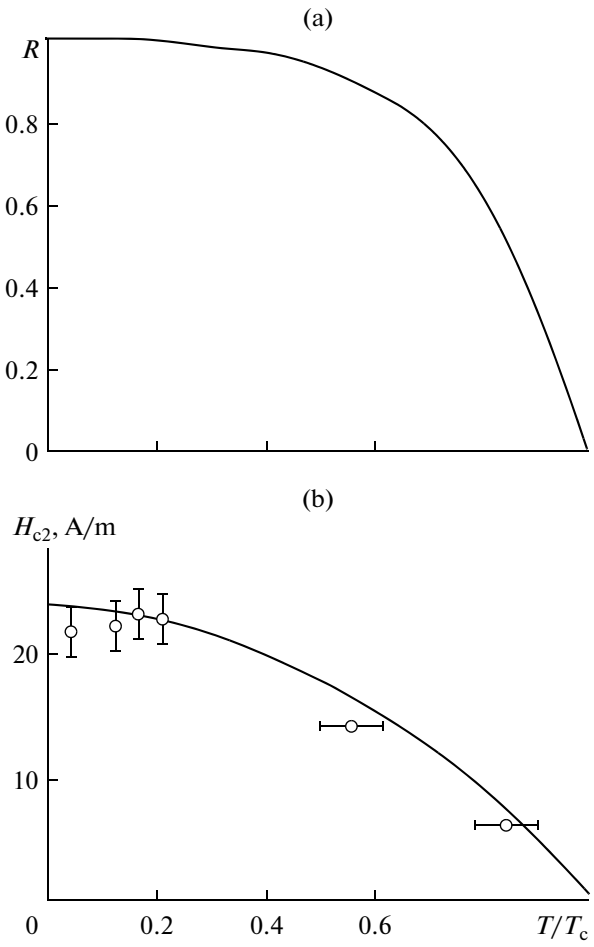

Fig. 12. (a) Possible change of order parameter R in the temperature range $0-T_c$ (see inset to Fig. 6) and (b) temperature dependence of upper critical field H_{c2} for YBaCuO HTSC [44].

A superdiamagnetization curve could qualitatively correspond to the curve shown in Fig. 12b, since the curve of a diamagnetic response has essentially the same character [45]. The relative diamagnetic response, i.e., $\bar{\lambda}_0/\lambda_T = 1$ at 0 K, and the character of its change with reduced temperature T/T_c coincide fully with the curve in Fig. 12b, and this dependence can also be approximately described by Tuin equation (9).

This consideration would not contradict the fact that, e.g., spontaneous magnetization is chosen as an order parameter to describe the phenomena related to magnetism. For example, the theory of zero-gap superconductivity does not need energy gap ε_g to consider damping in the temperature range T_c–0 K and an order–disorder transition.

CONCLUSIONS

(1) The results of measuring the elastic constants of niobium in the temperature range 77–625 K showed

that the anomaly of the temperature dependence of elastic constant c_{44} is also observed for polycrystalline niobium. Elastic instability is reflected on damping curves. The calculated temperature dependence of bulk modulus B allowed an assumption to be made about its role in superconductivity. Based on calculated data on the elastic and electron wavelengths, we assumed that they are in resonance at critical temperature T_c, which leads to the generation of a superconducting state in niobium.

(2) The elastic constants of yttrium ceramic $YBa_2Cu_3O_7$ were measured in the temperature ranges 295–77 and 295–800 K. Anomalies in damping and properties were detected in the temperature range 295–77 K. The change in Young's modulus in the range 295–800 K was shown to reflect an order–disorder transition in the ceramic.

(3) Critical Debye temperature $\bar{\theta}_D$, bulk modulus B, and longitudinal elastic modulus E_L were calculated for the temperature range 77–300 K. Based on the calculated data on the acoustic wavelengths, we proposed a mechanism for the appearance of superconductivity and the character of the order–disorder transition in yttrium ceramic $YBa_2Cu_3O_7$.

REFERENCES

1. J. Bardeen, "Electron-phonon interactions and superconductivity," Science **181** (4106), 1209–1214 (1973).
2. L. Pauling, "A resonating-valence-bond theory of metals and intermetallic compounds," Proc. Royal Soc. London. Ser. A. Mathem. Phys. Sci. **196** (1046), 343–362 (1949).
3. L. Pauling, "Influence of valence, electronegativity, atomic radii, and crest-trough interaction with phonons on the high-temperature copper oxide superconductors," Phys. Rev. Lett. **59**, 225–227 (1987).
4. Ya. I. Frenkel', *Introduction to the Theory of Metals* (Fizmatlit, Moscow, 1958).
5. J. Blakemor, *Solid State Physics* (Mir, Moscow, 1988).
6. J. M. Ziman, *Principles of the Theory of Solids* (University Press, Cambridge, 1964).
7. A. Animalu, *Intermediate Quantum Theory of Crystalline Solids* (Prentice-Hall, Englewood Cliffs, 1977).
8. M. V. Sadovskii, "High-temperature superconductivity in iron-based layered compounds," Usp. Fiz. Nauk **178** (12), 1243–1271 (2008).
9. O. K. Belousov and N. A. Palii, "On the problem of the superconducting transition temperature," Russian Metallurgy (Metally), No. 7, 526–544 (2012).
10. E. Walker, "Anomalous temperature behaviour of the shear elastic constant c_{44} in vanadium," Solid State Commun. **28** (7), 587–589 (1978).
11. E. Walker and P. Bujard, "Anomalous temperature behaviour of the shear elastic constant c_{44} in tantalum," Solid State Commun. **34** (8), 691–693 (1980).
12. P. Bujard, R. Sanjines, E. Walker, J. Ashkenazi, and M. Peter, "Elastic constants in Nb–Mo alloys from zero temperature to the melting point: experiment and theory," J. Phys. F.: Metal Phys. **11** (4), 775 (1981).
13. V. V. Struzhkin, Y. A. Timofeev, R. J. Hemley, and H. K. Mao, "Superconducting T_c and electron–phonon coupling in Nb to 132 GPa: magnetic susceptibility at megabar pressures," Phys. Rev. Lett. **79** (21), 4262 (1997).
14. A. Rogachev, A. T. Bollinger, and A. Bezryadin, "Influence of high magnetic fields on the superconducting transition of one-dimensional Nb and MoGe nanowires," Phys. Rev. Lett. **94** (1), 017004 (2005).
15. G. W. Crabtree, D. H. Dye, D. P. Karim, D. D. Koelling, and J. B. Ketterson, "Anisotropic many-body effects in the quasiparticle velocity of Nb," Phys. Rev. Lett. **42** (6), 390 (1979).
16. C. M. Varma and W. Weber, "Phonon dispersion in transition metals," Phys. Rev. B **19**, 6142–6154 (1979).
17. H. W. Weber, E. Seidl, C. Laa, E. Schachinger, M. Prohammer, A. Junod, and D. Eckert, "Anisotropy effects in superconducting niobium," Phys. Rev. B **44** (14), 7585 (1991).
18. *Physical Acoustics. Vol. 3. Lattice Dynamics*, Ed. by U. Meson (Mir, Moscow, 1968).
19. O. K. Belousov, "On the problem of estimating the theoretical mode I and shear strengths of crystals," Izv. Ross. Akad. Nauk, Ser. Met., No. 4, 56–65 (1999).
20. M. le Tacon, A. Bosak, S. M. Souliou, G. Dellea, T. Loew, R. Heid, and B. Keimer, "Inelastic X-ray scattering in $YBa_2Cu_3O_6$ reveals giant phonon anomalies and elastic central peak due to charge-density-wave formation," Nature Phys. **10** (1), 52–58 (2014).
21. H. M. Ledbetter, M. W. Austin, S. A. Kim, and M. Lei, "Elastic constants and Debye temperature of polycrystalline $Y_1Ba_2Cu_3O_{7-x}$," J. Mater. Res. **2** (6), 786–789 (1987).
22. H. M. Ledbetter, M. W. Austin, S. A. Kim, T. Datta, and C. E. Violet, "Shear-modulus change below T_c in $YBa_2Cu_3O_{7-x}$," J. Mater. Res. **2** (6), 790–792 (1987).
23. H. Ledbetter, "Elastic properties of metal-oxide superconductors," J. Minerals, Metals and Materials Soc. **40** (1), 24–30 (1988).
24. S. Huimin, W. Yening, Z. Zhifang, Z. Shiyuan, and S. Linhai, "A study of pseudo-elasticity in the superconducting oxide $YBa_2Cu_3O_{7-\delta}$," J. Phys. C : Solid State Phys. **20** (32), L889 (1987).
25. S. Bhattacharya, M. J. Higgins, D. C. Johnston, A. J. Jacobson, J. P. Stokes, J. T. Lewandowski, and D. P. Goshorn, "Anomalous ultrasound propagation in the high-T_c superconductors: $La_{1.8}Sr_{0.2}CuO_{4-y}$ and $YBa_2Cu_3O_{7-\delta}$," Phys. Rev. B **37** (10), 5901 (1988).
26. A. Migliori, T. Chen, B. Alavi, and G. Grüner, "Ultrasound anomaly at T_c in $YBa_2Cu_3O_y$," Solid State Commun. **63** (9), 827–829 (1987).
27. H. Kamioka, N. Okuda, and S. Nitta, "Elastic anomalies of high-T_c superconductor $YBa_2Cu_3O_{7-x}$ between 77 K and 300 K," Jap. J. Appl. Phys. **30** (6), 1204–1208 (1991).
28. J. Jiang, H. Yin, X. Wang, Y. Sun, F. Zeng, and J. Du, "Dependence of internal friction and Young's modulus on the oxygen deficiency in the superconductor $YBa_2Cu_3O_{7-\delta}$," Mater. Sci. Eng. B **7** (3), 227–230 (1990).
29. W. Yening, S. Huimin, Z. Jinsong, X. Ziran, M. Gu, N. Zhongmin, and Z. Zhifang, "Study on the anoma-

lies of $YBa_2Cu_3O_{9-x}$ between 90 and 260 K by elasticity measurements and X-ray diffraction," J. Phys. C: Solid State Phys. **20** (26), L665 (1987).

30. J. Toulouse, X. M. Wang, and D. J. L. Hong, "Ultrasonic evidence for a structural phase transition at 220 K in $YBa_2Cu_3O_{7-\delta}$," Phys. Rev. B **38** (10), 7077 (1988).
31. A. Balagurov, L. Mamsurova, I. Bobrikov, et al., "Effects of structural disordering in fine-grained $YBa_2Cu_3O_y$ HTSC," ZhETF **141** (6), 1144–1155 (2012).
32. O. K. Belousov, "Elastic constants and plasticity of Cu–Zn alloys," Russian Metallurgy (Metally), No. 1, 98–104 (2001).
33. L. Girifalco, *Statistical Physics of Materials* (Wiley, New York, 1973).
34. L. D. Landau and E. M. Lifshits, *Statistical Physics* (Nauka, Moscow, 1976).
35. O. K. Belousov "On the nature of the enthalpy of melting of metals," Izv. Ross. Akad. Nauk, Ser. Met., No. 3, 29–34 (1993).
36. A. Novik and B. Berry, *Relaxation Phenomena in Crystals* (Atomizdat, Moscow, 1975).
37. F. Blatt, *Physics of Electronic Conduction in Solids* (New York, 1968).
38. W. E. Alnaser, M. M. Zein, M. N. Khan, S. S. Al-Dallal, A. M. Memon, and M. J. Al-Othman, "The mechanical and structural properties of $Y_1Ba_2Cu_3O_{7-x}$ superconductors," J. Mater. Sci. **29** (2), 482–485 (1994).
39. R. Srinivasan, K. S. Girirajan, V. Ganesan, V. Radhakrishnan, and G. S. Rao, "Anomalous variation of the *c* lattice parameter of a sample of $YBa_2Cu_3O_{7-\delta}$ through the superconducting transition," Phys. Rev. B **38** (1), 889 (1988).
40. H. M. Ledbetter and S. A. Kim, "Hysteretic phase transition in $Y_1Ba_2Cu_3O_{7-x}$ superconductors," Phys. Rev. B **38** (16), 11857 (1988).
41. K. E. Uiks and F. E. Blok, *Thermodynamic Properties of 65 Elements, Their Oxides, Halides, Carbides, and Nitrides* (Metallurgiya, Moscow, 1965).
42. V. M. Pan, "Critical currents in high-T_c superconductors," ZhVKhO **34** (4), 509–518 (1989).
43. A. A. Abrikosov, "Second-order superconductors and a vortex lattice," Usp. Fiz. Nauk **174** (11) (2004).
44. G. Grissonnanche, Cyr-Choinière, O. Laliberfei, F. de Cotret, S.R. Juneau-Fecteau, A.S. Dufour-Beauséjour, and L. Taillefer, "Direct measurement of the upper critical field in a cuprate superconductor," Nature Commun. **5**, 1–8 (2014).
45. P. G. de Gennes, *Superconductivity of Metals and Alloys* (W. A. Benjamin, New York, 1966).

Translated by K. Shakhlevich